Comparison among multi-chain models for entangled polymer dynamics

Yuichi Masubuchi[1]* and Takashi Uneyama[2]
[1]Department of Mateirals Physics and [2]Center for Computational Science, Nagoya University, Japan.

ABSTRACT
Although lots of coarse-grained models have been proposed to trace long time behavior of entangled polymers, compatibility among different models has not been frequently discussed. In this study, the multi-chain slip-link model (primitive chain network model) and multi-chain slip-spring model have been examined for some dynamical and static measures, such as diffusion, relaxation modulus, chain dimension, entanglement density and the results have been compared with those reported for the standard bead-spring model. For the diffusion, three models are compatible with scaling parameters for unit of length, time and molecular weight. The relaxation modulus is also compatible given that the model dependence is accommodated for the entanglement density and the unit modulus. The chain dimension is in reasonable coincidence with small deviations due to the weak non-Gaussianity for the bead-spring model. Apart from these plausible compatibility, significant discrepancy has been found for the inter-chain cross-correlations in the relaxation modulus.

KEYWORDS
Bead-spring simulations, slip-link model, slip-spring model, viscoelasticity, multi-scale simulations

*To whom correspondence should be addressed
e-mail mas@mp.pse.nagoya-u.ac.jp
Tel +81-51-7892551

Soft Matter, 14, 29, 2018, 5986-5994

INTRODUCTION

Owing to the industrial significance as well as scientific interests, modeling of entangled polymer dynamics has been widely attempted[1]. Although molecular dynamics simulations are straightforward to trace molecular motion, the slow relaxation nature of the system does not allow practical calculations even for coarse-grained bead-spring models[2]. Smart idea is single chain modeling in which multi-chain effects are embedded into motional constraints with mean-field manner. In particular, the tube model[3] and its extensions have attained remarkable success. However, the drawback of this approach is difficulties for extensions toward complex systems, which are actually targeted for molecular simulations that take account of multi-body effects explicitly.

Motivated by the situation mentioned above, several coarse-grained multi-chain models have been proposed in between bead-spring models and tube models. Such models can be classified into two categories with respect to the modeling of entanglement. The rigorous approach is to prohibit chain crossing. Padding and Briels[4] have proposed the model referred as Twentanglement, in which the chain crossing is prohibited geometrically not relying on excluded volume interactions. Similar attempts for dissipative particle dynamics simulations[5] have been made by introducing the segmental repulsive potential[6]. The other direction is to mimic the entanglement effect by artificial settings. The multi-chain slip-link model, so-called primitive chain network model[7], is the realization of network consisting of a lot of reptating chains that are bundled by slip-links in pair at the entanglement points. Multi-chain slip-spring models[8–11] are inspired by the single-chain slip-spring model[12], in which the entanglement is reproduced by virtual springs that slide along the chain. Kindt and Briels[13] have developed a model so-called responsive particle dynamics to reproduce the entanglement effect by inter-particle interactions.

Although the abovementioned models have been evaluated with respect to comparison with experimental data, comparison among the models is also necessary. Coarse-grained models cannot recover short time dynamics and small structures according to the model constructions, whereas finely described models such as atomistic models cannot trace long time phenomena with practical calculation cost. To overcome such difficulties, multi-scale approaches have been attempted by combining a few different molecular models[14–17]. For this strategy, equality is assumed among the employed models in the overlapping domain for spatial and temporal scales. In this respect, a few critical tests have been reported for entangled polymer dynamics. Sukumaran and Likhtman[18] attempted to reproduce the segmental mean-square-displacement in bead-spring simulations by the single-chain slip-spring model. They have found that colored stochastic force is necessary for the single chain model rather than the usually employed white noise, for the matching of chain dynamics.

Takahashi et al[19] have reported the comparison between atomistic simulations of polyethylene and bead-spring simulations for the scaling behaviors of molecular weight dependence of static and dynamic measures. Their results have revealed that the scaling behavior around the onset of entanglement is not the same. These studies reveal the applicable range of bridging between the models, as well as possibility of further improvements for coarse-grained models. Nevertheless, tests for the assumed equivalence among the models are necessary.

In this study, a few multi-chain models are compared for the entangled polymer dynamics. The earlier data for the standard bead-spring model proposed by Kremer and Grest[2] were extracted for the diffusion and the viscoelastic relaxation to be used as the benchmark. The dynamical measures were compared to the results for the multi-chain slip-link model[7] and the multi-chain slip-spring model[8]. The scaling factors for length, time and molecular weight were determined from the diffusion. With the obtained scaling factors, coincidence for relaxation modulus was confirmed. However, for the contribution of inter-chain cross-correlation in the relaxation modulus, a strong model dependence was observed. Details are shown below.

MODELS AND SIMULATIONS

In this study, multi-chain slip-link and slip-spring simulations were performed. Since the details for both models can be found in the earlier publications[7,8,20], a brief description is given below. In the multi-chain slip-link model (referred to as primitive chain network model PCN, hereafter), entangled polymers are replaced by a network consisting of network strands, nodes and dangling ends. Each polymer is represented by a path between two dangling ends through the strands. At the nodes, two polymer segments are bundled via slip-link, which allows the chain sliding along its backbone whereas it restricts the perpendicular motion. The dynamics of the system is described by kinetic equations that take into account of drag force from the medium, force balance around entanglement, osmotic force suppressing density fluctuations and random force representing thermal agitations. When the chain penetrates out from the slip-link as a result of the sliding dynamics, the slip-link is removed and the chains are released. Conversely, when the chain end protrudes from the slip-link beyond a certain amount, a new slip-link is created by hooking another segment from the surroundings. In the multi-chain slip-spring model (MCSS hereafter), a lot of Rouse chains are dispersed in a simulation box. The chains are randomly connected by virtual springs that mimic entanglements. The virtual springs slides along the chain, and they are created/destructed at the chain ends, both according to detailed balance on the basis of the well-defined free energy.

For the PCN simulations, unit of length, time and energy is the average segment length a_{PCN}, the

diffusion time of the network node τ_{PCN}, and thermal energy $k_{\mathrm{B}}T$. τ_{PCN} is defined as $\tau_{\mathrm{PCN}} \equiv \zeta_{\mathrm{PCN}} a_{\mathrm{PCN}}^2 / 6k_{\mathrm{B}}T$, where ζ_{PCN} is the segment friction. For the MCSS simulations, unit of length and time is defined with a similar manner and denoted as a_{MCSS} and τ_{MCSS}. The unit of energy is $k_{\mathrm{B}}T$.

For both models, simulations in quiescent state were performed with periodic boundary conditions. The simulation time was at least 10 times longer than the longest relaxation time for each system. The simulation box size was sufficiently larger than the chain dimension. Typically, the simulation box accommodated 800 chains for PCN simulations and 200 chains for MCSS simulations. For the PCN simulations, the segment number density was 10 and the osmotic parameter was 0.5 in the PCN unit mentioned above. For the MCSS simulations, the segment number density was 4 in the MCSS unit and the chemical potential of slip-spring $\exp(\nu/kT)$ was 0.036. This number gives 3.5 beads between anchoring points along the chain on average. Periodic boundary condition was used with the box size sufficiently larger than the chain dimension. For statistics 8 independent simulation runs starting from different initial configurations were conducted.

The results of simulations mentioned above were compared to literature data collected for the standard Kremer-Grest model (KG hereafter), for which unit of length is the Lenard-Jones length σ and unit of energy is $k_{\mathrm{B}}T$. Unit of time τ is the standard time unit for Lennard-Jones liquids. The bead density is 0.85 and the temperature is 1.0. The static and dynamic measures discussed below will be shown in KG units unless stated.

RESULTS AND DISCUSSION

Figure 1 left panel shows the center-of-mass diffusion D as a function of bead number per chain N in KG units. All the simulation data indicate the expected power-law like behavior, for which the power-law exponent is -1 in the unentangled regime and is roughly -2 for N beyond the onset of entanglement[3]. For further critical comparison, Figure 1 right panel shows DN^2 where the diffusion is rescaled with respect to the prediction from the classical tube theory, as proposed by Likhtman[12]. In this plot, the Rouse behavior appears as the positive slope (with the exponent of unity) and the tube behavior corresponds to a horizontal line. As reported earlier for experimental data[21], the power-law exponent for diffusion constant with respect to the molecular weight is lower than -2 so that in Fig 1 right panel a negative slope appears in high molecular weight regime, following a peak. Consequently, DN^2 shows a convex curve with respect to N, and such a behavior can be confirmed for all the models. For very large N, PCN and MCSS predict a plateau like behavior that hints the classical tube behavior with the exponent of -2. Although further calculations for longer chains are necessary, this behavior is consistent with some experimental data, as summarized by Likhtman[12].

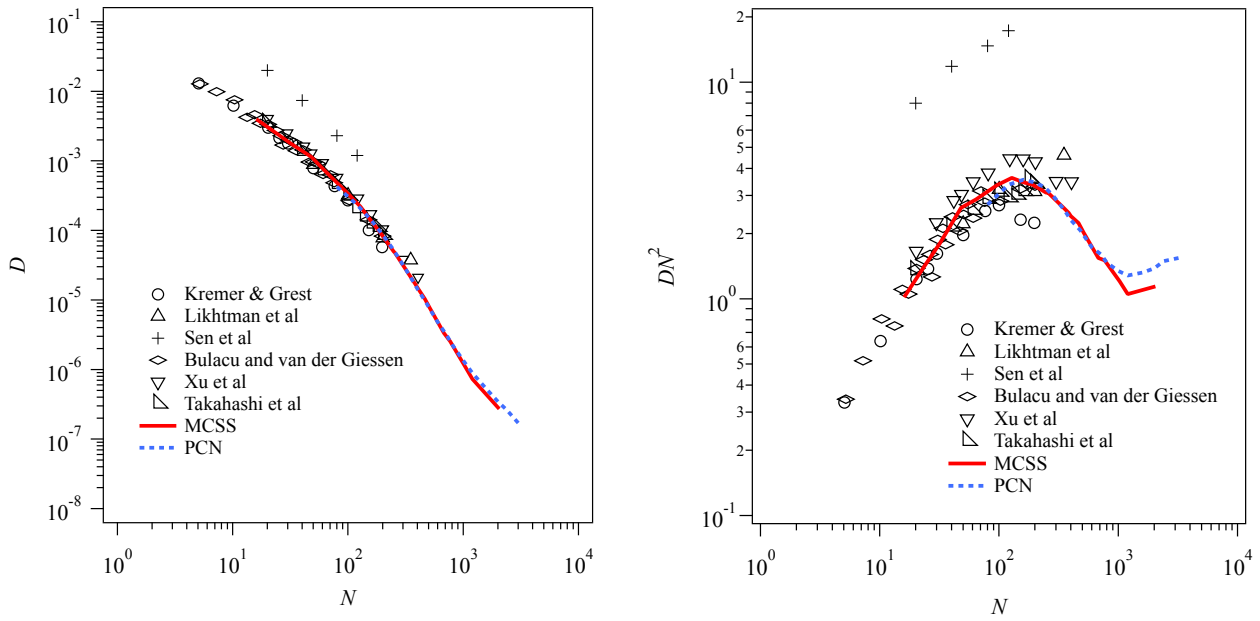

Figure 1 Diffusion coefficient (left) and its normalized value with respect to the classical reptation behavior (right) plotted against molecular weight. Red solid and blue dotted curves are the results of MCSS and PCN. KG results obtained from the literature[2,22–26] are shown by symbols.

Ideally, the resultant convex curve can be used for unequivocal comparison among the data. However, as shown in the figure, the bead-spring results are rather scattered for DN^2 whereas the difference is concealed in D. (For both plot, the data reported by Sen et al are very different from the others and they seem beyond possible statistical errors.) The scaling factors for PCN and MCSS for the data shown in Fig 1 were thus determined by the fitting for the mean-square-displacement (MSD) for the monomers around chain center $g_1(t)$ for the chains corresponding to $N = 50$, 100, 200 and 350 for KG shown in Fig 2. As described by the tube theory, $g_1(t)$ shows a series of power-law behaviors with changing the exponent, and the characteristic times can be determined from the transitions[3]. Namely, in the time scale shorter than τ_e, which is the Rouse time for the chain corresponding to the entanglement molecular weight, the exponent is 1/2. Between τ_e to τ_R, which is the Rouse time of the examined chain, it is 1/4. After τ_R, the exponent becomes 1/2 up to τ_d, which is the longest relaxation time. In the long time range beyond τ_d the exponent is unity showing the normal diffusion. These transitions have been reported for KG as seen in Fig 2 left panel, and the transitions in the long time regime are reproduced by PCN and MCSS, although the PCN result for the longest chain slightly underestimates the KG one reported by Likhtman et al. For comparison between different models with further clarity, in Fig 2 right panel $g_1(t)$ is multiplied by $t^{-1/2}$ as suggested by Likhtman. In this plot, the KG data from the other literatures are also shown, and the deviation of PCN from KG for the longest chain is within the scattering among KG data. The scattering of KG data probably indicates differences in the employed codes, initial configurations and number of chains. Nevertheless, the coincidence among different models is reasonably attained.

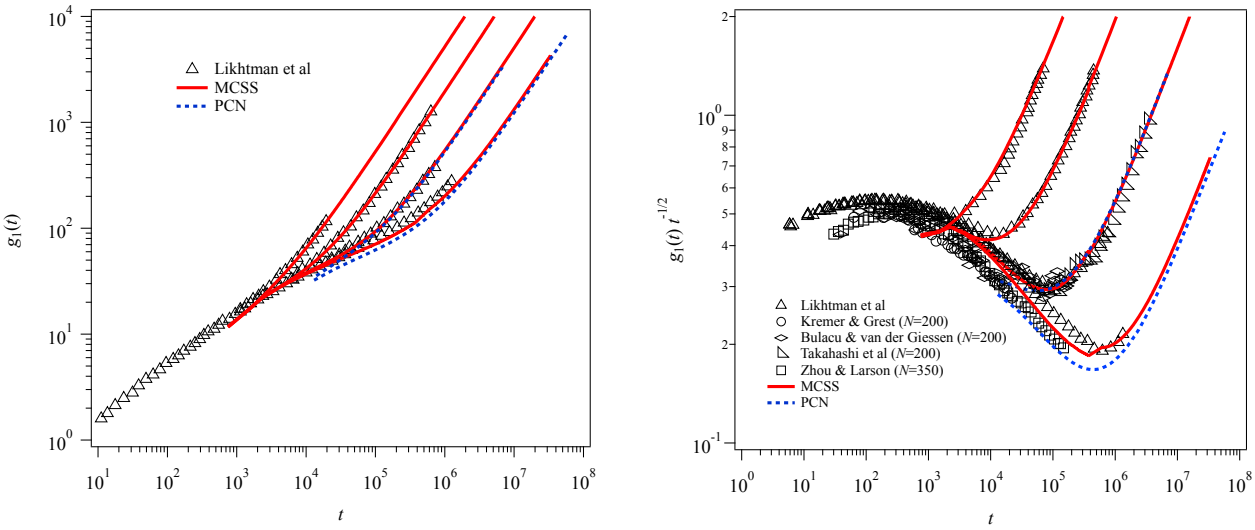

Figure 2 Time development of mean-squared-displacement of central monomers (left) and its normalized value with respect to the Rouse behavior (right) for $N = 50, 100, 200$ and 350. Red solid and blue dotted curves are for MCSS and PCN. Symbols are for KG extracted from the literature[2,22,24,26,27].

The comparison for diffusion unequivocally determines the scaling factors for molecular weight, time and length. The scaling factors thus determined are as follows:

$$N_{\mathrm{PCN}} = 5N_{\mathrm{MCSS}} = 40N \qquad (1)$$

$$a_{\mathrm{PCN}} = 2.0a_{\mathrm{MCSS}} = 6.2\sigma \qquad (2)$$

$$\tau_{\mathrm{PCN}} = 17\tau_{\mathrm{MCSS}} = 1.3 \times 10^4\tau \qquad (3)$$

Here, N_{PCN} and N_{MCSS} are the segment numbers per chain for PCN and MCSS, respectively.

For checking consistency between the scaling factors for length and molecular weight, the squared end-to-end distance $\mathbf{R}^2$ is shown in Figure 3 left panel in KG unit. Apparently there exist differences among the models owing to the difference in the chain stiffness. For further clarity, in Fig 3 right panel $\mathbf{R}^2$ is divided by N. As reported earlier[28], KG shows the non-Gaussian behavior for the short chains even with the screening of excluded volume interaction. For the coarse-grained models no excluded volume interaction is considered and the behaviors are close to Gaussian. Although $\mathbf{R}^2$ has the distribution (shown for MCSS by error-bar), the deviation between KG and the other models is not negligible. To eliminate the deviations, inter-beads interactions for the coarse-grained models have to be carefully designed on the basis of compressibility[29]. It should be also noted that the bead density must be carefully accommodated. Careful bridging attempts between atomistic molecular simulations and multi-chain slip-spring simulations have been recently reported on the basis of designed coarse-grained potentials obtained by the Boltzmann inversion scheme[30].

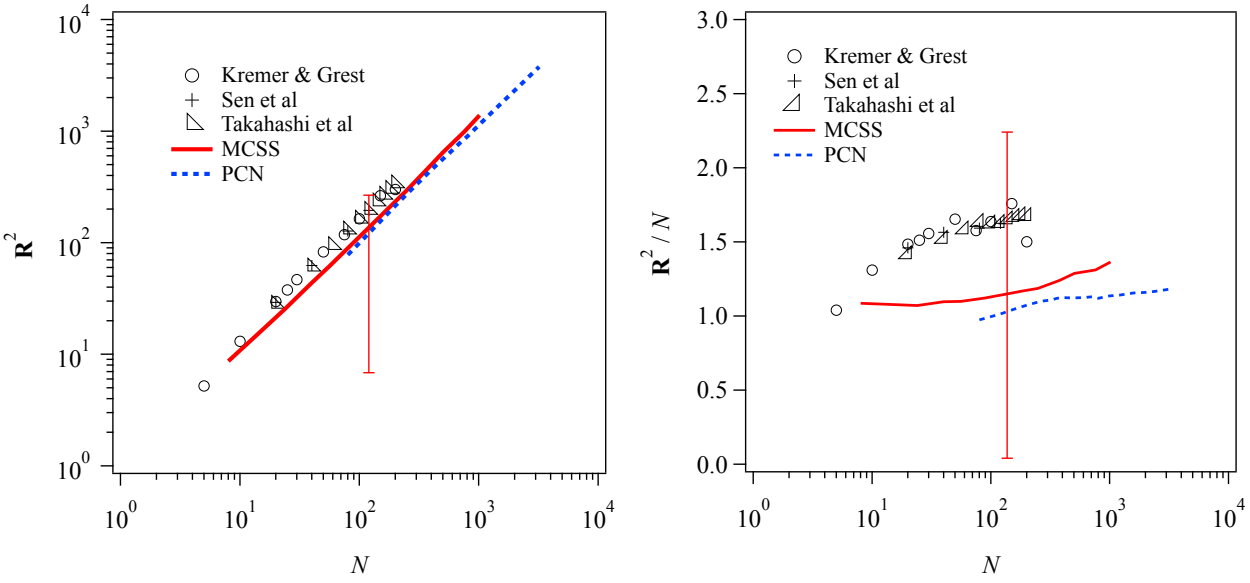

Figure 3 Squared end-to-end distance (left) and its normalized value with respect to the ideal chain statistics (right) plotted against molecular weight. Red solid and blue dotted curves are for MCSS and PCN. Symbols are for KG extracted from the literature. Error bar shows the distribution.

Although the scaling parameters for relevant units have been determined from MSD, for rheological calculations, scaling parameters for stress-optical coefficient is necessary and it must be determined from rheological response. For this sake, Figure 4 shows the comparison for linear relaxation modulus $G(t)$ obtained from the stress fluctuation by the Green-Kubo formula. In this comparison, the temporal scaling factor given by eq 3 is used, whereas the scaling for modulus is made to attain the best fit to the KG results reported by Likhtman et al[22]. For further clarity for the entanglement plateau, Fig 4 right panel shows $G(t)t^{1/2}$, in which $G(t)$ is normalized with respect to the Rouse behavior, for which $G(t) \propto t^{-1/2}$ before the terminal flow behavior. As reported earlier, the KG results for long chains clearly exhibit upward deviations from the Rouse behavior showing the effect of entanglement. These KG results are nicely reproduced by the coarse-grained models for the long chains. From the comparison, the scaling for modulus can be determined as follows;

$$G_{\mathrm{PCN}} = 3.9 \times 10^{-1} G_{\mathrm{MCSS}} = 1.9 \times 10^{-2} G_{\mathrm{KG}} \qquad (4)$$

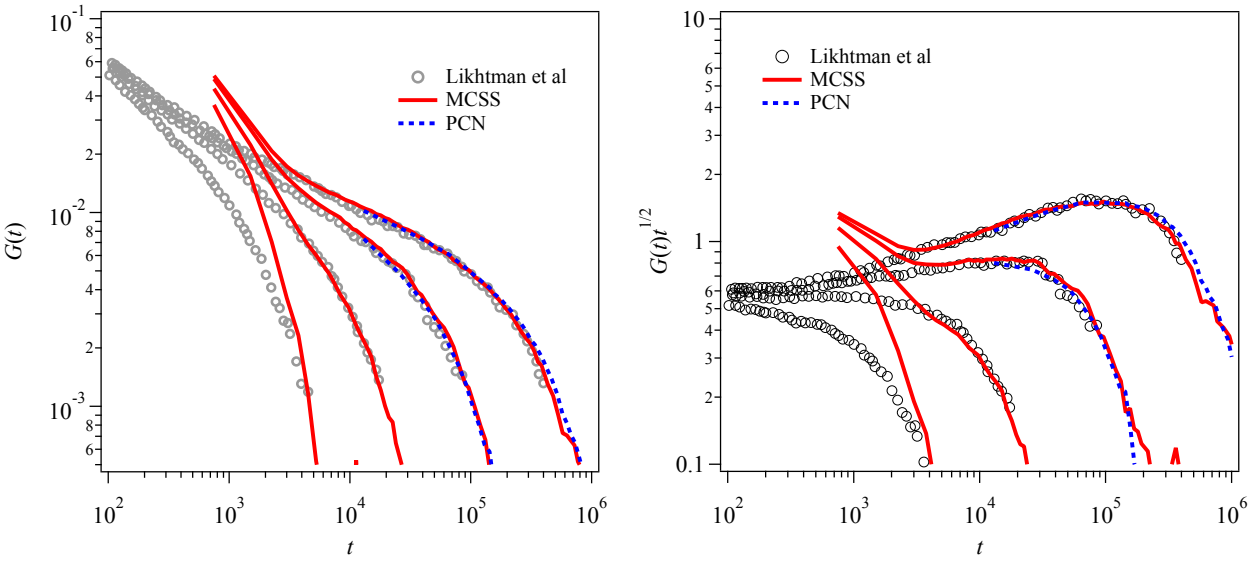

Figure 4 Linear relaxation modulus (left) and its normalized value with respect to the Rouse behavior (right) for $N = 50, 100, 200$ and 350. Red solid and blue dotted curves are for MCSS and PCN. Symbols are for KG results reported by Likhtman et al[22].

The relation shown in eq 4 can be related to the entanglement molecular weight. Figure 5 shows the entanglement molecular weight for KG, for which several different values have been reported as summarized by Moreira et al[31]. In most of literatures the entanglement molecular weight is reported as the Kuhn length of the primitive path, which is obtained from the primitive path analysis[32]. Following the expression by Everaers[33], the value obtained by this definition is referred as N_e^{PPKuhn}. N_e^{PPKuhn} increases with increasing N and saturates at $N_e^{\mathrm{PPKuhn}} \sim 90$ for $N > 1000$. The other definition of entanglement molecular weight is the topological-based one N_e^{topo}, which is determined by the network structure obtained by Z1 code[34] or CReTA code[35]. Hoy et al[36] have reported N_e^{topo} of KG for various molecular weights. As seen in Fig 5, N_e^{topo} steeply decreases and reaches a steady value for $N > 100$ at $N_e^{\mathrm{topo}} \sim 50$. Everaers[33] proposed the relation between N_e^{PPKuhn} and N_e^{topo}, and for the binary assumption of entanglement $N_e^{\mathrm{PPKuhn}} = 2N_e^{\mathrm{topo}}$, which is roughly consistent with Fig 5. Nevertheless, as discussed by Everaers[33], the networks in the slip-link and slip-spring models are topological-based and to be compared with N_e^{topo}. The value from PCN is according to eq 1, for which $N_e^{\mathrm{PCN}} = 1 = 40N$ and shown by horizontal dotted line in Fig 5. For MCSS, the value is calculated from the relation shown in eq 1 and the actual number of slip-springs in the system attained by the given value of $\exp(\nu/kT)$. Because the number of slip-springs is weakly molecular weight dependent, the MCSS value slightly increases with increasing molecular weight, and saturates around $N_e^{\mathrm{MCSS}} = 28N$. The relation among entanglement molecular weights for large N limit is thus summarized as below.

$$\frac{1}{N_e^{PCN}} = \frac{7 \times 10^{-1}}{N_e^{MCSS}} = \frac{2.5 \times 10^{-2}}{N_e^{topo}} \qquad (5)$$

The prefactors in eq 5 are similar to, but different from those in eq 4. The difference for prefactors is owing to the difference of chain density and difference of fluctuations imposed to the network nodes[37]. For PCN and MCSS, the magnitude of fluctuations is determined *a priori*. Specifically, for these models the friction coefficients for the segment motion and for the kinetics of topological constraint along the chain are different parameters from each other, and the ratio between two frictions has been arbitrarily chosen. The consistency for eqs 4 and 5 would be a possible guide for the tuning of frictions, whereas recent attempts have been reported for the friction determined from atomistic simulations[29,30]. For the entanglement structure, the distributions for N_e^{topo} must be discussed in addition to its average value. Although the consistency for PCN and MCSS with atomistic simulations has been reported[38,39], distributions for the standard KG simulations have not been reported in our knowledge and no comparison can be made at this time being.

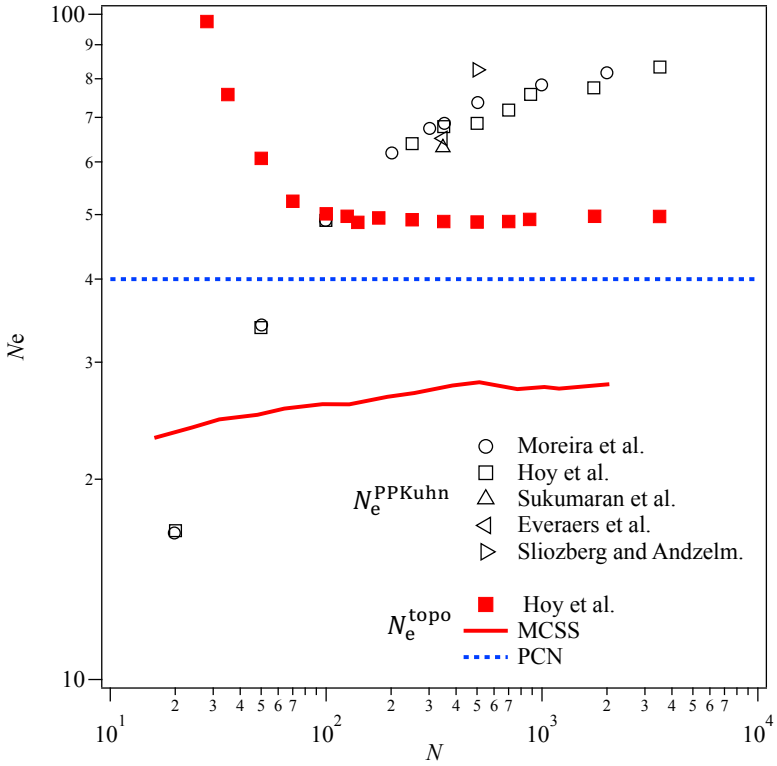

Figure 5 Entanglement molecular weight plotted against chain molecular weight. Red solid and blue dotted curves are for MCSS and PCN. Symbols are KG results from the literature[31,36,40], and filled and unfilled ones are for N_e^{topo} and N_e^{PPKuhn}, respectively.

For the comparison among the models, inter-chain cross-correlation is an interesting issue[41]. Although the chain dynamics is assumed to be independent in the single chain modeling, multi-chain

models have shown non-negligible amount of cross-correlations. Indeed, for KG, the cross-correlation has been discussed from a few different approaches[22,42–44]. In this specific study, the coupling parameter introduced by Cao and Likhtman is discussed. The coupling parameter $\kappa(t)$ is the ratio of cross-correlation contribution to the entire relaxation modulus. Recalling the success of single chain models, one may suppose that $\kappa(t)$ is close to zero or rapidly relaxes. However, $\kappa(t)$ grows with time and reaches ca. 50% of the total relaxation modulus for KG, as shown in Fig 6. For the coarse-grained models, growth of $\kappa(t)$ is also observed[45], including the upturn around the terminal time. However, the magnitude depends on the model and no universality is found here. Masubuchi and Amamoto[46] have shown that the magnitude of $\kappa(t)$ slightly depends on the incompressibility for PCN. Their result suggest that the tuning of inter-beads interactions for the coarse-grained models would compensate the discrepancy in $\kappa(t)$. However, such a modification for the models may disturb the consistencies for the other dynamical measures. Nevertheless, further studies for $\kappa(t)$ including that for bead-spring simulations are apparently necessary.

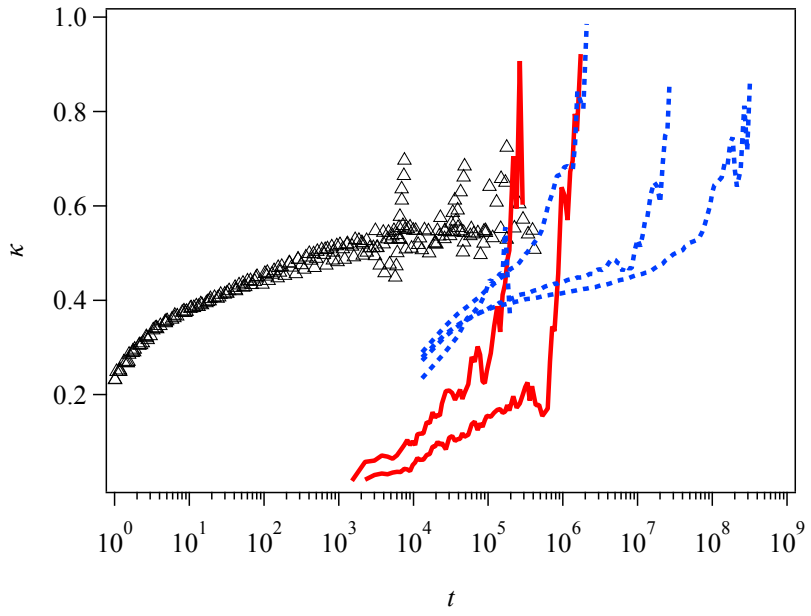

Figure 6 Time development of coupling parameter for inter-chain cross-correlations for $N = 50, 100, 200$ and 350. Red solid and blue dotted curves are for MCSS and PCN. Symbols are for KG results reported by Cao and Likhtman[44].

CONCLUSIONS

Detailed comparison has been performed among multi-chain models for dynamical and static measures for entangled polymers. As reported, all the models nicely exhibit the established universal behaviors for dynamical measures such as diffusion and relaxation modulus. Owing to the universality, the scaling factors were reasonably determined for molecular weight, time, length and

modulus. For chain dimension, small inconsistencies were observed due to the weak non-Gaussian nature of KG and lack of tunings for inter-beads potentials in coarse-grained models. Apart from the plausible results mentioned above, non-universal behaviors were found for the inter-chain cross-correlation for the relaxation modulus.

The results of this study confirm applicability of multi-scale strategies that rely on the universality of dynamic and static measures for entangled polymers. In particular, for the dynamical measures coincidence is attainable even without detailed tuning for model parameters. Meanwhile, it has been revealed that the significant inconsistency for inter-chain cross-correlation is concealed. Because inter-chain cross-correlations are difficult measure for experiments, further studies are apparently necessary for different multi-chain models. The other issue to be clarified is the compatibilities among the models under strong deformations and flows. Studies in such directions are being conducted and the results will be published elsewhere.

ACKNOWLEDGEMENT

This study is supported in part by Grant-in-Aid for Scientific Research (A) (17H01152) and for Scientific Research on Innovative Areas (18H04483) from JSPS. The support is also made by Council for Science, Technology and Innovation, Cross-ministerial Strategic Innovation Promotion Program, "Structural Materials for Innovation" from JST.

REFERENCES

[1] Y. Masubuchi, Annu. Rev. Chem. Biomol. Eng. **5**, 11 (2014).

[2] K. Kremer and G.S. Grest, J. Chem. Phys. **92**, 5057 (1990).

[3] M. Doi and S.F. Edwards, *The Theory of Polymer Dynamics* (Clarendon press, Oxford, 1986).

[4] J.T. Padding and W.J. Briels, J. Chem. Phys. **115**, 2846 (2001).

[5] F. Lahmar, C. Tzoumanekas, D.N. Theodorou, and B. Rousseau, Macromolecules **42**, 7485 (2009).

[6] S. Kumar and R.G. Larson, J. Chem. Phys. **114**, 6937 (2001).

[7] Y. Masubuchi, J.-I.I. Takimoto, K. Koyama, G. Ianniruberto, G. Marrucci, and F. Greco, J. Chem. Phys. **115**, 4387 (2001).

[8] T. Uneyama and Y. Masubuchi, J. Chem. Phys. **137**, 154902 (2012).

[9] V.C. Chappa, D.C. Morse, A. Zippelius, and M. Müller, Phys. Rev. Lett. **109**, 148302 (2012).

[10] A. Ramírez-Hernández, F.A. Detcheverry, B.L. Peters, V.C. Chappa, K.S. Schweizer, M. Müller, and J.J. de Pablo, Macromolecules **46**, 6287 (2013).

[11] M. Langeloth, Y. Masubuchi, M.C. Böhm, and F. Müller-plathe, J. Chem. Phys. **138**, 104907

(2013).
[12] A.E. Likhtman, Macromolecules **38**, 6128 (2005).
[13] P. Kindt and W.J. Briels, J. Chem. Phys. **127**, 134901 (2007).
[14] K. Kremer and F. Müller-Plathe, MRS Bull. **26**, 205 (2001).
[15] F. Müller-Plathe, F. Müller-Plathe, and F. Müller-Plathe, ChemPhysChem **3**, 754 (2002).
[16] V.A. Harmandaris, N.P. Adhikari, N.F.A. Van Der Vegt, and K. Kremer, Macromolecules **39**, 6708 (2006).
[17] P.S. Stephanou, C. Baig, and V.G. Mavrantzas, Soft Matter **7**, 380 (2011).
[18] S.K. Sukumaran and A.E. Likhtman, Macromolecules **42**, 4300 (2009).
[19] K.Z. Takahashi, R. Nishimura, N. Yamato, K. Yasuoka, and Y. Masubuchi, Sci. Rep. **7**, 12379 (2017).
[20] Y. Masubuchi, G. Ianniruberto, F. Greco, and G. Marrucci, Model. Simul. Mater. Sci. Eng. **12**, S91 (2004).
[21] T.P. Lodge, Phys. Rev. Lett. **83**, 3218 (1999).
[22] A.E. Likhtman, S.K. Sukumaran, and J. Ramirez, Macromolecules **40**, 6748 (2007).
[23] S. Sen, S.K. Kumar, and P. Keblinski, Macromolecules **38**, 650 (2005).
[24] M. Bulacu and E. Van Der Giessen, J. Chem. Phys. **123**, (2005).
[25] X. Xu, J. Chen, and L. An, J. Chem. Phys. **142**, 74903 (2015).
[26] K.Z. Takahashi, N. Yamato, K. Yasuoka, and Y. Masubuchi, Mol. Simul. **43**, (2017).
[27] Q. Zhou and R.G. Larson, Macromolecules **40**, 3443 (2007).
[28] R. Auhl, R. Everaers, G.S. Grest, K. Kremer, and S.J. Plimpton, J. Chem. Phys. **119**, 12718 (2003).
[29] G.G. Vogiatzis, G. Megariotis, and D.N. Theodorou, Macromolecules **50**, 3004 (2017).
[30] A.P. Sgouros, G. Megariotis, and D.N. Theodorou, Macromolecules **50**, 4524 (2017).
[31] L.A. Moreira, G. Zhang, F. Müller, T. Stuehn, and K. Kremer, Macromol. Theory Simulations **24**, 419 (2015).
[32] R. Everaers, S.K. Sukumaran, G.S. Grest, C. Svaneborg, A. Sivasubramanian, and K. Kremer, Science (80-.). **303**, 823 (2004).
[33] R. Everaers, Phys. Rev. E - Stat. Nonlinear, Soft Matter Phys. **86**, 1 (2012).
[34] M. Kroger, Comput. Phys. Commun. **168**, 209 (2005).
[35] C. Tzoumanekas and D.N. Theodorou, Macromolecules **39**, 4592 (2006).
[36] R.S. Hoy, K. Foteinopoulou, and M. Kr??ger, Phys. Rev. E - Stat. Nonlinear, Soft Matter Phys. **80**, 14 (2009).
[37] Y. Masubuchi, G. Ianniruberto, F. Greco, and G. Marrucci, J. Chem. Phys. **119**, 6925 (2003).
[38] Y. Masubuchi, T. Uneyama, H. Watanabe, G. Ianniruberto, F. Greco, and G. Marrucci, J. Chem. Phys. **132**, 1 (2010).

[39] A. Ramírez-Hernández, B.L. Peters, M. Andreev, J.D. Schieber, and J.J. De Pablo, J. Chem. Phys. **143**, (2015).

[40] Y.R. Sliozberg and J.W. Andzelm, Chem. Phys. Lett. **523**, 139 (2012).

[41] A.E. Likhtman, J. Nonnewton. Fluid Mech. **157**, 158 (2009).

[42] J. Gao and J.H. Weiner, J. Chem. Phys. **91**, 3168 (1989).

[43] J. Ramírez, S.K. Sukumaran, and A.E. Likhtman, J. Chem. Phys. **126**, (2007).

[44] J. Cao and A.E. Likhtman, Phys. Rev. Lett. **104**, 207801 (2010).

[45] Y. Masubuchi and S.K. Sukumaran, Nihon Reoroji Gakkaishi **41**, 1 (2013).

[46] Y. Masubuchi and Y. Amamoto, Nihon Reoroji Gakkaishi **44**, 219 (2016).